Infiltration of Solution-Processable Solid Electrolytes into Conventional Li-Ion-Battery Electrodes for All-Solid-State Li-Ion Batteries

Dong Hyeon Kim,[†] Dae Yang Oh,[†] Kern Ho Park,[†] Young Eun Choi,[†] Young Jin Nam,[†] Han Ah Lee,[†] Sang-Min Lee,[‡] and Yoon Seok Jung*,[†]

[†]School of Energy and Chemical Engineering, Department of Energy Engineering, Ulsan National Institute of Science and Technology (UNIST), Ulsan 44919, South Korea

[‡]Battery Research Center, Korea Electrotechnology Research Institute, 12 Bulmosan-ro 10 beon-gil, Changwon 642-120, South Korea

S Supporting Information

ABSTRACT: Bulk-type all-solid-state lithium-ion batteries (ASLBs) have the potential to be superior to conventional lithium-ion batteries (LIBs) in terms of safety and energy density. Sulfide SE materials are key to the development of bulk-type ASLBs because of their high ionic conductivity (max of $\sim 10^{-2}$ S cm^{-1}) and deformability. However, the severe reactivity of sulfide materials toward common polar solvents and the particulate nature of these electrolytes pose serious complications for the wet-slurry process used to fabricate ASLB electrodes, such as the availability of solvent and polymeric binders and the formation of ionic contacts and networks. In this work, we report a new scalable fabrication protocol for ASLB electrodes using conventional composite LIB electrodes and homogeneous SE solutions (Li$_6$PS$_5$Cl (LPSCl) in ethanol or 0.4LiI−0.6Li$_4$SnS$_4$ in methanol). The liquefied LPSCl is infiltrated into the tortuous porous structures of LIB electrodes and solidified, providing intimate ionic contacts and favorable ionic percolation. The LPSCl-infiltrated LiCoO$_2$ and graphite electrodes show high reversible capacities (141 and 364 mA h g^{-1}) at 0.14 mA cm^{-2} (0.1 C) and 30 °C, which are not only superior to those for conventional dry-mixed and slurry-mixed ASLB electrodes but also comparable to those for liquid electrolyte cells. Good electrochemical performance of ASLBs employing the LPSCl-infiltrated LiCoO$_2$ and graphite electrodes at 100 °C is also presented, highlighting the excellent thermal stability and safety of ASLBs.

KEYWORDS: All-solid-state batteries, lithium-ion batteries, solid electrolytes, solution-process, electrodes, infiltration, coatings, sulfides
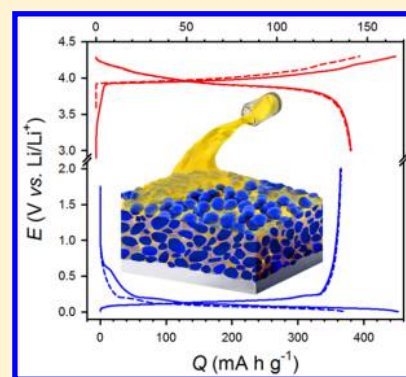
Lithium-ion battery (LIB) technology currently faces two critical challenges: serious safety concerns associated with flammable liquid electrolytes (LEs) and high energy density, especially for applications in electric vehicles. Solidifying electrolytes have emerged as a very promising solution to these problems.[1−8] Inorganic solid electrolytes (SEs) are nonflammable and have the potential to work with Li metal, which is the ultimate anode material for high-energy density.[3−10] Moreover, the use of SEs enables the minimization of inactive components such as packaging material because an increased battery pack voltage can be achieved by stacking bipolar electrodes.[5,11] Among the various potential candidates for all-solid-state lithium-ion batteries (ASLBs), composite-structured bulk-type ASLBs employing sulfide SEs are very competitive because of their practicability and promising electrochemical performance.[3−7,12] Sulfide materials can form two-dimensional contacts with active materials by a simple mechanical pressing process.[8,11,13,14] In contrast, fabrication of composite electrodes employing brittle oxide SE materials such as Li$_7$La$_3$Zr$_2$O$_{12}$ require high-temperature sintering processes, which inevitably result in large interfacial impedances.[15−17] Moreover, there has been noticeable progress in the ionic

conductivity of sulfide materials (e.g., Li$_{10}$GeP$_2$S$_{12}$:[3] 12 mS cm^{-1}; Li$_7$P$_3$S$_{11}$:[4] 17 mS cm^{-1}; and Li$_{9.54}$Si$_{1.74}$P$_{1.44}$S$_{11.7}$Cl$_{0.3}$:[5] 25 mS cm^{-1}).

Recently, solution-based syntheses for various sulfide SE materials have attracted much attention. A report about β-Li$_3$PS$_4$ showing 0.16 mS cm^{-1}, synthesized from Li$_2$S and P$_2$S$_5$ in tetrahydrofuran[18] ignited explosive interest in this field. Subsequent developments include Li$_3$PS$_4$ (0.0026 mS cm^{-1} using N-methylformamide),[19] Li$_7$P$_2$S$_8$I (0.63 mS cm^{-1} using acetonitrile),[20] 0.4LiI-0.6Li$_4$SnS$_4$ (0.41 mS cm^{-1} using methanol (MeOH)),[8] Li$_6$PS$_5$Cl (LPSCl) (0.014 mS cm^{-1} using ethanol (EtOH)),[21] Na$_3$SbS$_4$ (0.1−0.2 mS cm^{-1} using water or MeOH),[14] and Li$_7$P$_3$S$_{11}$ (1.5 mS cm^{-1} using acetonitrile).[22] Our group demonstrated that the use of homogeneous SE solutions enabled the direct coating of highly conductive solidified electrolytes onto active materials for all-solid-state Li- and Na-ion batteries using 0.4LiI-0.6Li$_4$SnS$_4$ and Na$_3$SbS$_4$,

respectively, thereby dramatically improving the rate capabilities as compared to conventionally mixed electrodes.[8,14]

In most previous reports, the fabrication of all-solid-state cells was based on tedious mixing of the active materials, SEs, and carbon additives in dry conditions.[3,5,6,11,12] However, from the perspective of practical applications, the addition of polymeric binders is essential to enable large roll-to-roll processable sheet-type electrodes to be obtained.[11] Thus, a wet-process using liquid solvents to dissolve the polymeric binders is necessary. Unfortunately, the severe reactivity of sulfide materials toward polar solvents prohibits the use of conventional polymeric binders (e.g., poly(vinylidene fluoride) (PVDF), poly(vinyl alcohol) (PVA), carboxymethyl cellulose (CMC)), and solvents (N-methyl-2-pyrrolidinone (NMP) and water).[23] Thus, the choice of solvents for the wet-processing of the sulfide-SE-based electrodes for ASLBs is restricted to nonpolar or very less polar aprotic solvents, such as toluene and xylene.[11,24,25] The availability of polymeric binders is thus highly limited; e.g., nitrile−butadiene rubber (NBR), styrene−butadiene rubber (SBR), and silicone rubber.[24,25] The slurry process for conventional LIB electrodes is a matter of homogeneously mixing three components (active materials, conducting additives, and binders) and focuses on the electrical wiring of the active materials. The use of a slurry process for ASLB electrodes requires the homogenization of four components (active materials, conducting additives, binders, and SEs). Thus, the slurry for ASLB electrodes should be optimized to achieve favorable conduction pathways for both electrons and Li$^+$ ions simultaneously, which increases the engineering costs. Overall, compared to the case for conventional LIB electrodes, the fabrication of ASLB electrodes is much more complicated because of the restricted choice of solvents and polymeric binders and by ionic percolations. Moreover, the use of SE particles in the fabrication process of electrodes poses the problem of poor ionic contacts, which could be addressed by the use of coatable and solution-processable SEs.[8,14]

Based on the aforementioned research and motivation, we report an alternative scalable fabrication protocol for ASLB electrodes that takes advantage of liquefied SEs to simply infiltrate conventional LIB electrodes with homogeneous SE solutions (Li$_6$PS$_5$Cl/EtOH or 0.4LiI−0.6Li$_4$SnS$_4$/MeOH). Our approach enables the adoption of the highly optimized electrode-fabrication protocols for conventional LIBs and allows wetting of the SEs onto the active materials and favorable ionic percolations. The LPSCl-infiltrated LiCoO$_2$ (LCO) and graphite (Gr) electrodes show reversible capacities of 141 mA h g^{-1} (3.0−4.3 V versus Li/Li$^+$) and 364 mA h g^{-1} (0.005−2.0 V versus Li/Li$^+$) at 0.14 mA cm^{-2} (0.1 C) at 30 °C, respectively, which are superior to those for the conventional dry- and slurry-mixed electrodes for ASLBs and comparable to those for LE cells. We also highlight that ASLBs assembled using the LPSCl-infiltrated LCO and Gr electrodes show good performance not only at 30 °C but also at 100 °C.

Among the wet chemistries of sulfide SEs developed so far,[8,18−21,26] the homogeneity of the LPSCl/EtOH and 0.4LiI−0.6Li$_4$SnS$_4$/MeOH solutions and the high conductivities of the resulting SEs (≥0.1 mS cm^{-1}) make these materials the only suitable candidates for the infiltration of LIB electrodes with SEs for ASLBs.[8,21] The LPSCl/EtOH solution was chosen because of its compatibility with the Al current collector and wide electrochemical window of the resulting LPSCl. LPSCl powders obtained by ball-milling the precursors (Li$_2$S, P$_2$S$_5$, and

LiCl), referred to as "BM-LPSCl," dissolved completely in anhydrous EtOH, forming a homogeneous solution (Figure S1a). The SE was obtained as pale white powder after evaporating the solvent under vacuum and a heat treatment at 180 °C under vacuum; these powders are referred to as "Sol-LPSCl" (Figure S1b). The XRD patterns for BM-LPSCl and Sol-LPSCl show the characteristic peaks of the argyrodite Li$_6$PS$_5$Cl (CIF no. 418490) without any impurity phases (Figure S2).[27] The Raman spectra for BM-LPSCl and Sol-LPSCl also reveal strong signatures from PS$_4^{3-}$, centered at 423 cm^{-1}.[21] The ionic conductivity of Sol-LPSCl, measured by AC impedance using symmetric Ti/SE/Ti cells, was 0.19 mS cm^{-1} at 30 °C (Figure S3). Further heat treatment of Sol-LPSCl at higher temperatures increased the ionic conductivity, hitting 1.0 mS cm^{-1} for the sample heat-treated at 550 °C (Table S1).[27] However, considering thermal stability of PVDF, the heat-treatment temperature for SE-infiltrated electrodes was fixed to be 180 °C.[28,29] The conductivity value of 0.19 mS cm^{-1} for the Sol-LPSCl heat-treated at 180 °C is high enough to operate all-solid-state batteries at room temperature.[8,14] The lower ionic conductivity of Sol-LPSCl heat-treated at 180 °C than that of BM-LPSCl or Sol-LPSCl heat-treated at 550 °C is considered to originate from trace amounts of organic impurities, as indicated by thermogravimetric analysis (TGA) results (Figure S4).[21]

The process for infiltration of conventional composite LIB electrodes (LCO and Gr electrodes) with solution-processable SEs is illustrated in Figure 1. The LIB electrodes were prepared by casting and spreading a slurry based on PVDF and NMP on the current collectors (Al and Ni foils for the LCO and Gr electrodes, respectively). The as-prepared LIB electrodes were infiltrated with the solution of LPSCl in EtOH by a dip-coating method, which could be replaced by more scalable coating methods for further development, such as spray-coating.[30] The subsequent removal of the solvent under an Ar atmosphere and heat treatment at 180 °C under vacuum caused solidified LPSCl layers to form on any exposed surfaces of the tortuous porous structures in the composite electrodes. It was found that porosities of the electrodes were thus decreased after the infiltration of SEs (prior to cold-pressing; Table 1). Finally, the SE-infiltrated electrodes were densified by cold-pressing under 770 MPa during the fabrication process for all-solid-state cells, ensuring more-intimate ionic contacts, as confirmed by very low porosities of 6−8%. Volumetric contributions from the infiltrated SEs and the pores give overall 29−34 vol % which is comparable to the porosity for the commercial LIB electrodes.[31] Moreover, the LPSCl-infiltrated LCO electrode hot-pressed under 460 MPa at 150 °C showed negligible porosity. The SE-infiltrated electrodes also retained good adhesion to the Al current collector after a bending test (Movie S1 and Figure S5), suggesting their applicability to the scalable roll-to-roll process.[11]

The Raman spectra and XRD patterns of the LCO and Gr electrodes were obtained before and after their infiltration with LPSCl to examine the compatibility of the active materials and the LPSCl solution (Figure 2a and b). In the Raman spectra for both LPSCl-infiltrated LCO and Gr electrodes, strong peaks are clearly seen for PS$_4^{3-}$ at 423 cm^{-1} (labeled "♦"); this result is identical to that for Sol-LPSCl (Figure S2b). The characteristic peaks of LiCoO$_2$ (A$_{1g}$ and E$_g$)[32] and graphite (D and G modes)[33] were also retained after the infiltration with LPSCl. The XRD patterns for LPSCl-infiltrated electrodes consistently showed signatures from crystalline Li$_6$PS$_5$Cl (labeled "*") and
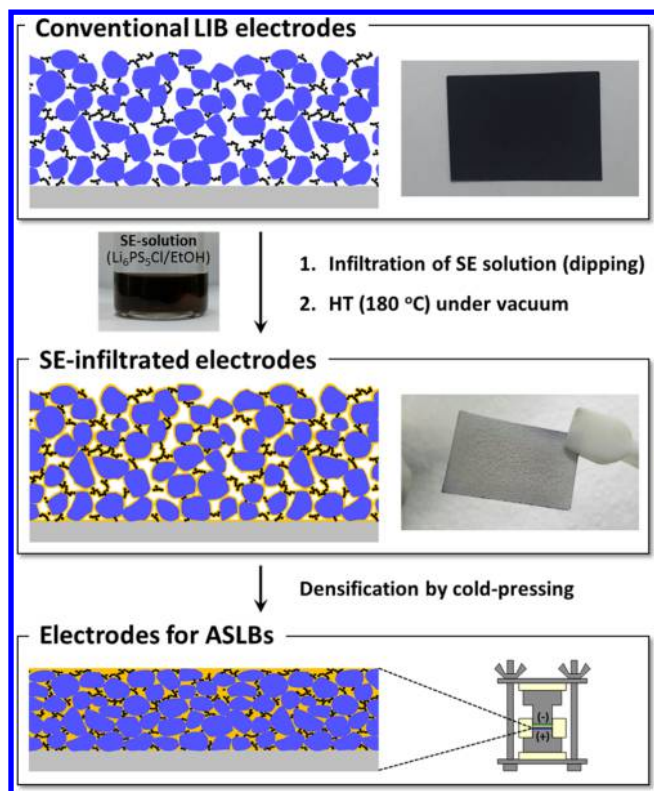
Figure 1. Schematic diagram illustrating the infiltration of conventional LIB composite electrodes with solution-processable SEs. The photographs in the panels show the LiCoO$_2$ electrodes before and after the infiltration of EtOH-solution processed Li$_6$PS$_5$Cl (LPSCl). A photograph of LPSCl-dissolved EtOH solution is also shown. Polymeric binders (PVDF) are not shown in the diagram for simplicity.

no changes in the peak positions for LiCoO$_2$ (labeled "&") and graphite (labeled "#") (Figures 2b and S6). It is therefore confirmed that the solidification of LPSCl is not affected by the presence of other electrode components and that the active materials (LCO and Gr) remain intact in contact with the LPSCl-dissolved EtOH solution.

A cross-sectional field-emission scanning electron microscopy (FESEM) image and its corresponding energy dispersive X-ray spectroscopy (EDXS) elemental maps for the LPSCl-infiltrated LCO electrode after densification are presented in Figures 2c and S7. In all of the cross-sectional surfaces, the SEs occupy the spaces between the active particles well, which is attributed to the excellent penetration by the liquefied SEs (SE solutions) and deformability of SEs. A high-resolution transmission electron microscopy (HRTEM) image and its corresponding EDXS elemental maps for a focused ion beam (FIB) cross-sectioned sample (Figure 2d) revealed the intimate contacts between LCO and LPSCl at a microscopic level, highlighting the importance of solution-processable SEs.[8,14] An even distribution of LPSCl was also confirmed for the densified LPSCl-infiltrated Gr electrode (Figure S8).

Electrochemical characterization of LPSCl-infiltrated LCO and Gr electrodes was carried out by using all-solid-state LCO/Li–In and Gr/Li–In half-cells at 30 °C (Figure 3). The first- and second-cycle charge–discharge voltage profiles of all-solid-state cells with LPSCl-infiltrated LCO and Gr electrodes at 0.14 mA cm^{-2} (∼0.1C) are shown in panels a and b of Figure 3, respectively. These results were compared with the results for the LE-cells, for which electrodes without SE infiltration were used. Note that the specifications used for the electrodes are realistic for practical applications. The compositions (active material/PVDF/Super P weight ratio) and mass loadings for the LCO and Gr electrodes (for the data in Figure 3a and b) are 97:1:2/10 mg$_{LCO}$ cm^{-2} and 95:5:0/6 mg$_{Gr}$ cm^{-2}, respectively (Table 1). The fractions of LPSCl after the infiltration were only 11 and 21 wt % for the LCO and Gr electrodes, respectively. The all-solid-state cell using the LCO electrode without SE infiltration exhibited negligible capacity (the inset in Figure 3a). In stark contrast, the SE-infiltrated LCO electrode prepared by cold-pressing (Figure 3a) or hot-pressing (Figure S9) showed a high reversible capacity of 141 mA h g^{-1} in the voltage range of 3.0–4.3 V (versus Li/Li$^+$), which is comparable to that for the LE-cell (154 mA h g^{-1}). Surprisingly, the reversible capacity of the LPSCl-infiltrated Gr electrode in the all-solid-state cell (364 mA h g^{-1}) exceeded that for the LE-counterpart (312 mA h g^{-1}) in the voltage range of 0.005–2.0 V (versus Li/Li$^+$). It is emphasized that the high capacities for the SE-infiltrated electrodes, along with the low porosities and the low volume fraction of inactive components (SEs, PVDF, and Super P; Table 1), indicate their competitiveness in volumetric energy density, compared with the conventional LIB electrodes.
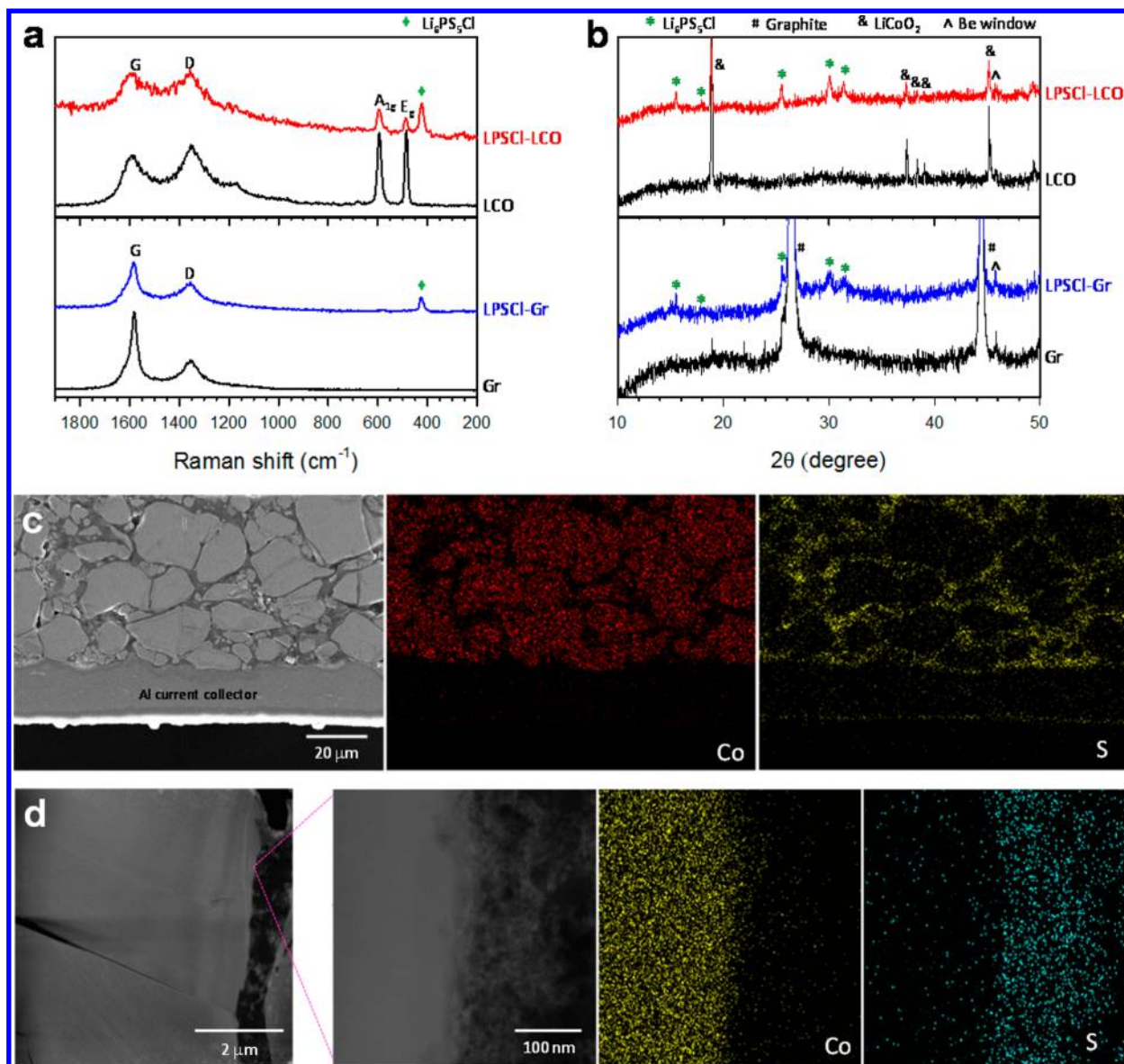
The SE-infiltrated LCO and Gr electrodes exhibited low first-cycle Coulombic efficiencies (CEs) of 76.6% and 80.7%, respectively (Table S2). As supported by theoretical calculations and evidenced by experiments, the sulfide SEs are not thermodynamically stable at low or high voltages.[34−37] Irreversible electrochemical insertion or extraction of Li$^+$ ions for the SEs in contact with active materials or current collectors for negative and positive electrodes, respectively, could take place.[34,35] However, formation of favorable decomposition products that are ionically conductive but electronically insulating and protective coatings on the surface of electrode

Table 1. Characteristics of LCO and Gr Electrodes for the Infiltration of SE (LPSCl)

| electrode | composition[a] | porosity (%) | | | fraction of SE | | surface coverage of SEs onto active materials (%)[b] |
| | | before SE infiltration | after SE infiltration | | (wt %) | (vol %) | |
			before cold-pressing	after cold-pressing			
LCO	96:2:2	54	29	7.3	12	26	56
	97:1:2	52	29	6.7	11	27	61
	98:1:1	53	27	6.3	12	27	65
Gr	95:5:0	50	35	7.1	21	22	—
	92:8:0	48	38	8.0	21	23	—

[a]Weight ratio of active material to PVDF to Super P. [b]Obtained by GITT analysis.
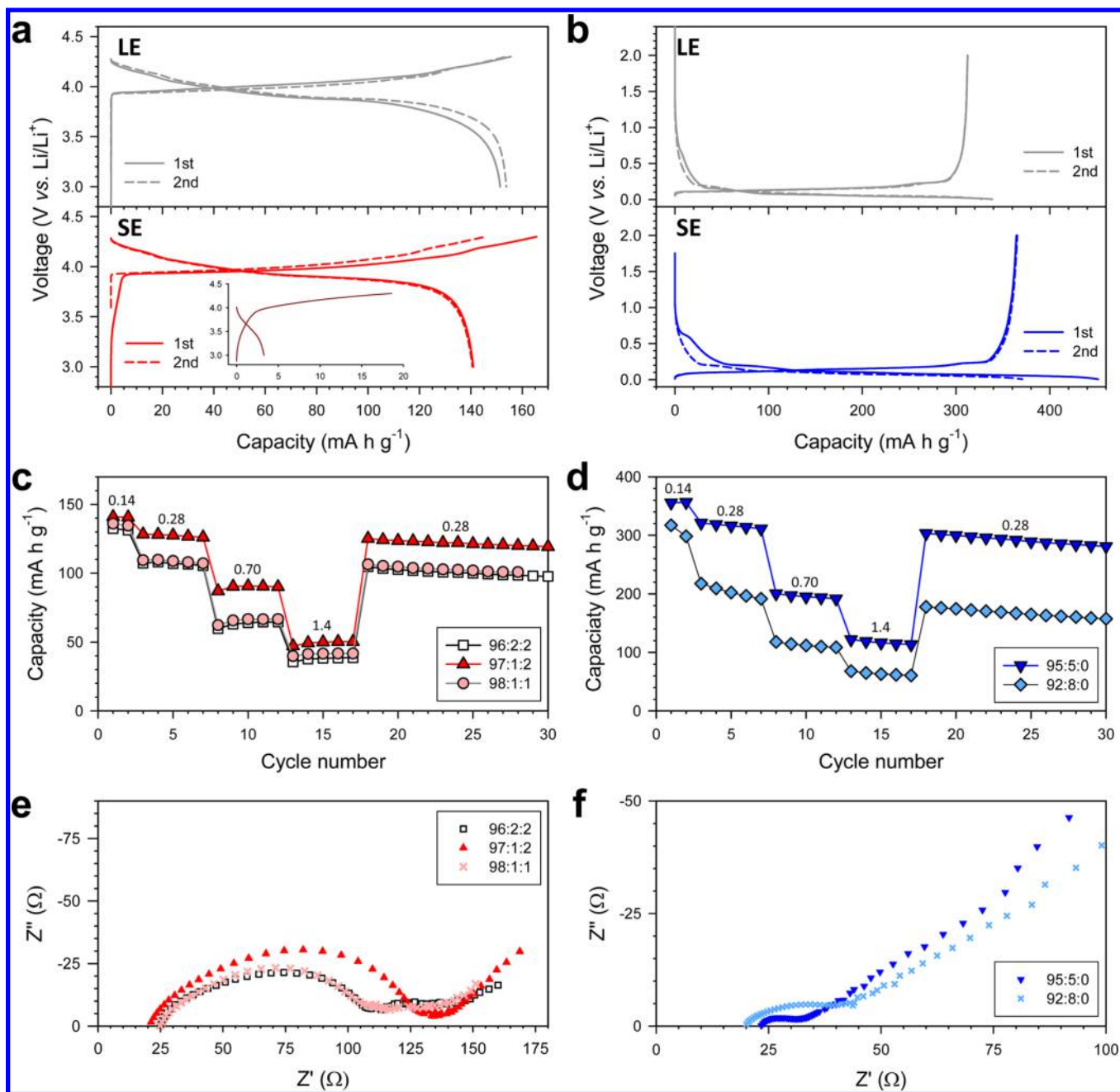
Figure 2. Characterization of SE (LPSCl)-infiltrated LiCoO$_2$ (LCO) and graphite (Gr) electrodes. (a) Raman spectra and (b) XRD patterns of LCO and Gr electrodes before and after the infiltration of solution-processed LPSCl. Signatures from LiCoO$_2$ (A$_{1g}$ and E$_g$ modes) and graphite (D and G bands) are shown in panel a. (c) Cross-sectional FESEM image of the LPSCl-infiltrated LCO electrode and its corresponding EDXS elemental maps. (d) HRTEM image of FIB-cross-sectioned LPSCl-infiltrated LCO electrode and its corresponding EDXS elemental maps.

materials could minimize the degradation and result in stable performances,[37,38] which is also the case for the conventional LIBs using LEs.[39]

The results for the electrodes fabricated by dry-mixing without binders (referred to as "Mixture1"), dry-mixing with the PVDF binder (referred to as "Mixture2"), and slurry-mixing with NBR binder and xylene (referred to as "Mixture3") were also compared (Figure S10 and Table S2). The SE-infiltrated LCO electrode (141 mA h g^{-1}) outperformed the Mixture1 electrode (135 mA h g^{-1}). Considering that the Mixture1 electrode is free from insulating polymeric binders, while the SE-infiltrated electrode includes a PVDF binder, the higher capacity for the latter is attributed to the more intimate ionic contacts between LCO and LPSCl enabled by the solution-processing of the SE.[8,14] The surface coverage of SE on the active material for the LPSCl-infiltrated LCO electrode, obtained by galvanostatic intermittent titration technique

(GITT) analysis,[8] was 61% (Figure S11 and Table 1). This value is two times higher than that of the conventional dry-mixed electrode (31%) reported in our previous work, in which no binders were used.[8] The capacity of the Mixture2 electrode was also lower (118 mA h g^{-1}) than that for the Mixture1 electrode, which is attributed to the ionically insulating property of PVDF. The Mixture3 electrode showed a reversible capacity of only 14 mA h g^{-1}. Combined with the effect of ionic blocking by the NBR binder, an uneven distribution of the four components (LCO, Super P, NBR, and LPSCl) in the slurry may have imbalanced the electronic and ionic conduction pathways in the Mixture3 electrode. These comparisons highlight the exceptional advantages of the infiltration of as-formed LIB electrodes with solution-processable SEs in terms of intimate ionic contact and favorable ionic percolation.

Figure 3c and d compare the reversible capacities of the LPSCl-infiltrated LCO and Gr electrodes at different current

Figure 3. Electrochemical characterization of all-solid-state LCO/Li−In and Gr/Li−In half-cells employing the LPSCl-infiltrated electrodes at 30 °C. First- and second-cycle charge−discharge voltage profiles of (a) LCO and (b) Gr electrodes at 0.14 mA cm^{-2} (∼0.1C) for liquid-electrolyte and all-solid-state cells. The result for the LCO electrode, which was an all-solid-state cell without infiltration of the SE, is shown in the inset of a). Rate performances of c) LCO and d) Gr electrodes in all-solid-state cells. The numbers indicate the current densities in mA cm^{-2}. The current densities for charge and discharge were the same. Nyquist plots for (e) LCO and (f) Gr electrodes in all-solid-state cells. The compositions of electrodes in terms of the weight ratio of active material/PVDF/Super P are shown in panels c−f.

densities (mA cm^{-2}), respectively, varied by electrode composition (LCO/PVDF/Super P weight ratio). The rate capabilities for the LCO and Gr electrodes were enhanced by decreasing the amount of PVDF (97:1:2 > 96:2:2 for LCO and 95:5:0 > 92:8:0 for Gr), which is attributed to improved ionic contact between LPSCl and the active materials. This conclusion is also supported by the higher surface coverage of SEs on LCO for the 97:1:2 (61%) composition than for the 96:2:2 (56%) composition (Table 1). However, despite achieving a further increase in surface coverage of SEs by decreasing the amount of Super P in the LCO electrode

(98:1:1, 65%), the rate capability decreased, which could be explained by insufficient electronic conduction pathways. The amplitude of the semicircles in the Nyquist plots (Figure 3e and f), which is associated with the contribution of ionic and electronic contacts in the electrode components,[8,14,40−42] also agrees well with the trends observed for the rate performances.

The LPSCl-infiltrated LCO and Gr electrodes cycled at 0.70 mA cm^{-2} (∼0.5C) and 0.28 mA cm^{-2} exhibited 88.6% and 86.1% capacity retention as compared to the capacity at the 3rd cycle after 50 and 100 cycles, respectively (Figure S12). The LCO electrode (without SE infiltration) in the conventional LE
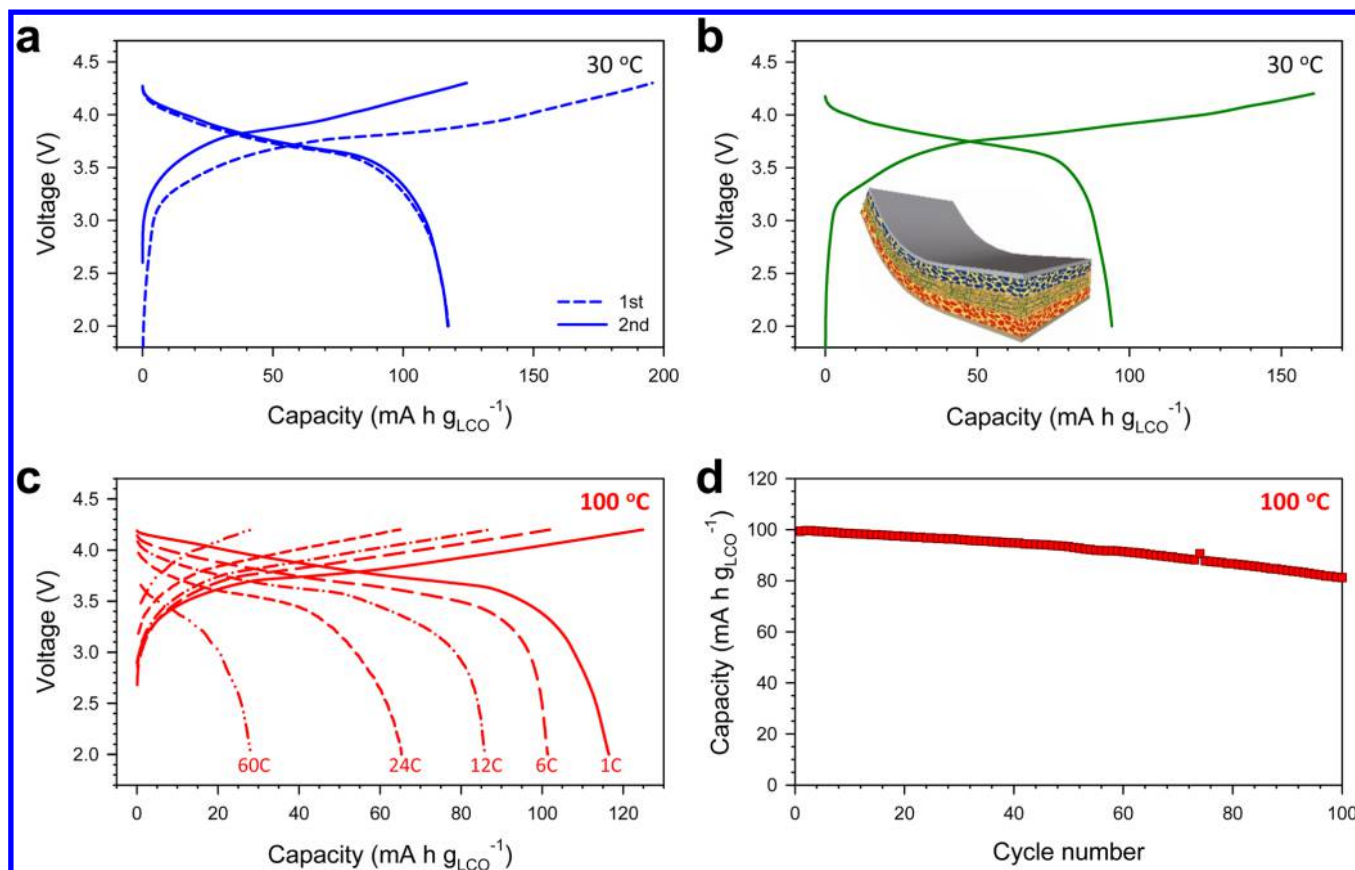
Figure 4. Electrochemical performances of LCO/Gr ASLBs employing LPSCl-infiltrated electrodes at 30 and 100 °C. Initial charge−discharge voltage profiles of LCO/Gr ASLB at 0.1C (0.14 mA cm^{-2}) and 30 °C using (a) a conventional thick (∼600 μm) SE layer (2.0−4.3 V) and (b) a thin (∼70 μm) SE−NW composite film (2.0−4.2 V). (c) Charge−discharge voltage profiles at different C-rates and (d) cycling performance at 6C for LCO/Gr ASLB at 100 °C (2.0−4.2 V).

cell showed 97.4% capacity retention after 50 cycles (Figure S13). The poorer cycling stability of LCO in the all-solid-state cell than in the LE cell is not surprising because LCO suffers from interfacial stability problem in contact with sulfide SEs, which could be explained by chemical reactions or interatomic diffusion[35,36,38] or by the space charge layer theory.[43] In this regard, a conformal Al_2O_3 coating as a protective layer has been applied on the as-formed LCO electrode by three cycles of atomic layer deposition (ALD) prior to the SE infiltration.[28,29] As compared to the bare LCO electrode, the Al_2O_3 ALD-coated electrode exhibited an improved capacity retention of 98.1% after 50 cycles. This preliminary result emphasizes the importance and promising opportunities on elaborative electrode−electrolyte interfacial engineering for ASLBs, which will be our next mission.

The infiltration of the LIB electrode with another solution-processable Li-ion SE, $0.4LiI−0.6Li_4SnS_4$, was also demonstrated (Figure S14). Despite conductivity of $0.4LiI−0.6Li_4SnS_4$ (0.41 mS cm^{-1}) being higher than that of solution-processed LPSCl (0.19 mS cm^{-1}), the $0.4LiI−0.6Li_4SnS_4$-infiltrated LCO electrode showed a lower reversible capacity (112 mA h g^{-1}) than its LPSCl-infiltrated counterpart (141 mA h g^{-1}). This difference was attributed to the corrosion of the Al current collector by contact with the $0.4LiI−0.6Li_4SnS_4$-dissolved MeOH solution (Figure S15).[44]

Finally, all-solid-state LCO/Gr full cells were assembled using the LPSCl-infiltrated LCO and Gr electrodes, and their charge−discharge voltage profiles are shown in Figure 4. The

LCO/Gr ASLB exhibited a reversible capacity of 117 mA h g$_{LCO}^{-1}$ at 0.1 C (0.14 mA cm^{-2}) in the voltage range of 2.0−4.3 V at 30 °C (Figure 4a), which corresponds to an energy density of 279 Wh kg$_{LCO+Gr}^{-1}$ or 213 Wh kg$_{electrodes}^{-1}$. The LCO/Gr full battery also showed good rate and cycling stability at 30 °C (Figure S16). The capacity retention at 1 C as compared to the capacity at 0.1 C was 81.7% and 51.4% with the constant charging-rate (0.1 C) and the same charge−discharge rate mode, respectively. After 79 cycles of charge−discharge at 0.5 C, the LCO/Gr full battery retained 95.9% of its initial capacity. Instead of the conventional thick SE layer (∼600 μm) (for the data in Figure 4a), a thin and bendable SE-nonwoven (NW) composite film (∼70 μm)[11] was also used between the LPSCl-infiltrated LCO and Gr electrodes. The LCO/Gr ASLB assembled with the SE-NW film exhibited 94 mA h g$_{LCO}^{-1}$ at 0.1C (0.14 mA cm^{-2}) between 2.0−4.2 V at 30 °C (Figure 4b). This proof-of-concept combination of the SE-infiltrated electrodes and a bendable and thin SE-NW film highlights the applicability of the as-developed ASLBs to roll-to-roll fabrication processes.[45] The performance of the LCO/Gr ASLB was also evaluated at 100 °C (Figure 4c and d), which is far beyond the operation temperature ranges for conventional LIBs.[5,46] The LCO/Gr ASLB showed a capacity of 65 mA h g$_{LCO}^{-1}$ at the high rate of 24 C (Figure 4c) and a capacity retention of 82% at 6 C after the 100th cycle (Figure 4d).

In comparison with the conventional LIB technology, the overall electrochemical performances (especially the rate capabilities) of ASLBs employing the LPSCl-infiltrated LCO

and Gr electrodes at 30 °C are not yet very impressive. However, it should be emphasized that a new proof-of-concept has been successfully demonstrated herein. We suggest that relevant future research directions are as follows. The development of new solution-processable SEs with higher ionic conductivity and good compatibility with electrode components are of prime importance. The development of functional polymeric binders would further improve the performance. For example, employing binders that form point contacts with active materials[47] or ionically conducting binders[48,49] could minimize the impedance at the SE−active materials interface. Finally, the infiltration of porous polymeric separators with solution-processable SEs would allow the manufacturing processes of conventional LIBs, for which the LEs are injected into the as-formed jelly rolls, to be fully adapted to production of ASLBs.[45] The ASLB could be activated by the injection of liquefied SEs into preassembled electrodes-separator assemblies and solidification, followed by densification.

In summary, a new scalable electrode-fabrication protocol for ASLBs was successfully demonstrated by infiltrating conventional LIB electrodes with solution-processable SEs (LPSCl or $0.4LiI−0.6Li_4SnS_4$). This process achieved intimate ionic contacts and favorable ionic percolation, which resulted in high reversible capacities of 141 and 364 mA h g^{-1} for the LPSCl-infiltrated LCO and Gr electrodes, respectively, at 0.14 mA cm^{-2} (0.1 C) and 30 °C. These values were comparable to those of LE cells and superior to those for conventional dry-mixed (with or without binders) and slurry-mixed (with NBR binder) all-solid-state cells. The electrode composition of the LIB electrodes prior to SE infiltration was found to affect their electrochemical performance in terms of the available electronic and ionic pathways. Finally, the LCO/Gr ASLBs with LPSCl-infiltrated electrodes demonstrated excellent performance at 100 °C as well as at 30 °C. Moreover, the demonstration of LCO/Gr ASLB, for which a thin and bendable SE−NW film was sandwiched between LPSCl-infiltrated electrodes, highlighted their applicability for production by roll-to-roll processes. We believe that our results pave a new way to practical all-solid-state battery technology.

ASSOCIATED CONTENT

Ⓢ Supporting Information

The Supporting Information is available free of charge on the ACS Publications website at DOI: 10.1021/acs.nanolett.7b00330.

> Experimental methods and supplementary results. Figures showing solution photographs, XRD and Raman spectra, an Arrhenius plot, TGA profiles, LPSCl-infiltrated LCO electrodes, FESEM images, EDXS elemental maps, voltage profiles, GITT results, cycling performances, experimental results, rate and cycling stability, experimental photographs, ionic conductivities, and a comparison of the electrochemical performances. (PDF)
>
> Movie showing LPSCl-infiltrated LCO electrodes for the bending test. (AVI)

AUTHOR INFORMATION

Corresponding Author

*E-mail: ysjung@unist.ac.kr.

ORCID Ⓞ

Yoon Seok Jung: 0000-0003-0357-9508

Author Contributions

The manuscript was written through contributions of all authors. All authors have given approval to the final version of the manuscript.

Notes

The authors declare no competing financial interest.

ABBREVIATIONS

LIB, lithium-ion battery; LE, liquid electrolyte; SE, solid electrolyte; ASLB, all-solid-state lithium-ion battery; LPSCl, Li_6PS_5Cl; EtOH, ethanol; MeOH, methanol; PVDF, poly-(vinylidene fluoride); CMC, carboxymethyl cellulose; NMP, N-methyl-2-pyrrolidinone; NBR, nitrile−butadiene rubber; SBR, styrene−butadiene rubber; LCO, $LiCoO_2$; Gr, graphite; TGA, thermogravimetric analysis; FESEM, field-emission scanning electron microscopy; EDXS, energy-dispersive X-ray spectroscopy; HRTEM, high-resolution transmission electron microscopy; FIB, focused ion beam; CE, Coulombic efficiency; GITT, galvanostatic intermittent titration technique; ALD, atomic layer deposition; NW, nonwoven

REFERENCES

(1) Goodenough, J. B.; Kim, Y. *Chem. Mater.* **2010**, *22*, 587−603.
(2) Tarascon, J.-M. *Philos. Trans. R. Soc., A* **2010**, *368*, 3227−3241.
(3) Kamaya, N.; Homma, K.; Yamakawa, Y.; Hirayama, M.; Kanno, R.; Yonemura, M.; Kamiyama, T.; Kato, Y.; Hama, S.; Kawamoto, K.; Mitsui, A. *Nat. Mater.* **2011**, *10*, 682−686.
(4) Seino, Y.; Ota, T.; Takada, K.; Hayashi, A.; Tatsumisago, M. *Energy Environ. Sci.* **2014**, *7*, 627−631.
(5) Kato, Y.; Hori, S.; Saito, T.; Suzuki, K.; Hirayama, M.; Mitsui, A.; Yonemura, M.; Iba, H.; Kanno, R. *Nat. Energy* **2016**, *1*, 16030.
(6) Jung, Y. S.; Oh, D. Y.; Nam, Y. J.; Park, K. H. *Isr. J. Chem.* **2015**, *55*, 472−485.
(7) Janek, J.; Zeier, W. G. *Nat. Energy* **2016**, *1*, 16141.
(8) Park, K. H.; Oh, D. Y.; Choi, Y. E.; Nam, Y. J.; Han, L.; Kim, J.-Y.; Xin, H.; Lin, F.; Oh, S. M.; Jung, Y. S. *Adv. Mater.* **2016**, *28*, 1874−1883.
(9) Wang, Y.; Richards, W. D.; Ong, S. P.; Miara, L. J.; Kim, J. C.; Mo, Y.; Ceder, G. *Nat. Mater.* **2015**, *14*, 1026−1032.
(10) Han, X.; Gong, Y.; Fu, K. K.; He, X.; Hitz, G. T.; Dai, J.; Pearse, A.; Liu, B.; Wang, H.; Rubloff, G.; Mo, Y.; Thangadurai, V.; Wachsman, E. D.; Hu, L. *Nat. Mater.* **2016**, DOI: 10.1038/nmat4821.
(11) Nam, Y. J.; Cho, S. J.; Oh, D. Y.; Lim, J. M.; Kim, S. Y.; Song, J. H.; Lee, Y. G.; Lee, S. Y.; Jung, Y. S. *Nano Lett.* **2015**, *15*, 3317−3323.
(12) Yersak, T. A.; Macpherson, H. A.; Kim, S. C.; Le, V. D.; Kang, C. S.; Son, S. B.; Kim, Y. H.; Trevey, J. E.; Oh, K. H.; Stoldt, C.; Lee, S. H. *Adv. Energy Mater.* **2013**, *3*, 120−127.
(13) Sakuda, A.; Hayashi, A.; Tatsumisago, M. *Sci. Rep.* **2013**, *3*, 2261.
(14) Banerjee, A.; Park, K. H.; Heo, J. W.; Nam, Y. J.; Moon, C. K.; Oh, S. M.; Hong, S.-T.; Jung, Y. S. *Angew. Chem., Int. Ed.* **2016**, *55*, 9634−9638.
(15) Kim, K. H.; Iriyama, Y.; Yamamoto, K.; Kumazaki, S.; Asaka, T.; Tanabe, K.; Fisher, C. A. J.; Hirayama, T.; Murugan, R.; Ogumi, Z. *J. Power Sources* **2011**, *196*, 764−767.
(16) Ohta, S.; Seki, J.; Yagi, Y.; Kihira, Y.; Tani, T.; Asaoka, T. *J. Power Sources* **2014**, *265*, 40−44.

(17) El-Shinawi, H.; Paterson, G. W.; MacLaren, D. A.; Cussen, E. J.; Corr, S. A. *J. Mater. Chem. A* **2017**, *5*, 319−329.

(18) Liu, Z.; Fu, W.; Payzant, E. A.; Yu, X.; Wu, Z.; Dudney, N. J.; Kiggans, J.; Hong, K.; Rondinone, A. J.; Liang, C. *J. Am. Chem. Soc.* **2013**, *135*, 975−978.

(19) Teragawa, S.; Aso, K.; Tadanaga, K.; Hayashi, A.; Tatsumisago, M. *J. Power Sources* **2014**, *248*, 939−942.

(20) Rangasamy, E.; Liu, Z.; Gobet, M.; Pilar, K.; Sahu, G.; Zhou, W.; Wu, H.; Greenbaum, S.; Liang, C. *J. Am. Chem. Soc.* **2015**, *137*, 1384−1387.

(21) Yubuchi, S.; Teragawa, S.; Aso, K.; Tadanaga, K.; Hayashi, A.; Tatsumisago, M. *J. Power Sources* **2015**, *293*, 941−945.

(22) Yao, X. Y.; Liu, D.; Wang, C. S.; Long, P.; Peng, G.; Hu, Y. S.; Li, H.; Chen, L. Q.; Xu, X. X. *Nano Lett.* **2016**, *16*, 7148−7154.

(23) Oh, D. Y.; Nam, Y. J.; Park, K. H.; Jung, S. H.; Cho, S.-J.; Kim, Y. K.; Lee, Y.-G.; Lee, S.-Y.; Jung, Y. S. *Adv. Energy Mater.* **2015**, *5*, 1500865.

(24) Inada, T.; Takada, K.; Kajiyama, A.; Kouguchi, M.; Sasaki, H.; Kondo, S.; Watanabe, M.; Murayama, M.; Kanno, R. *Solid State Ionics* **2003**, *158*, 275−280.

(25) Ito, S.; Fujiki, S.; Yamada, T.; Aihara, Y.; Park, Y.; Kim, T. Y.; Baek, S.-W.; Lee, J.-M.; Doo, S.; Machida, N. *J. Power Sources* **2014**, *248*, 943−950.

(26) Wang, Y.; Liu, Z.; Zhu, X.; Tang, Y.; Huang, F. *J. Power Sources* **2013**, *224*, 225−229.

(27) Deiseroth, H.-J.; Kong, S.-T.; Eckert, H.; Vannahme, J.; Reiner, C.; Zaiss, T.; Schlosser, M. *Angew. Chem., Int. Ed.* **2008**, *47*, 755−758.

(28) Jung, Y. S.; Cavanagh, A. S.; Riley, L. A.; Kang, S. H.; Dillon, A. C.; Groner, M. D.; George, S. M.; Lee, S. H. *Adv. Mater.* **2010**, *22*, 2172−2176.

(29) Jung, Y. S.; Cavanagh, A. S.; Gedvilas, L.; Widjonarko, N. E.; Scott, I. D.; Lee, S. H.; Kim, G. H.; George, S. M.; Dillon, A. C. *Adv. Energy Mater.* **2012**, *2*, 1022−1027.

(30) Pasquarelli, R. M.; Ginley, D. S.; O'Hayre, R. *Chem. Soc. Rev.* **2011**, *40*, 5406−5441.

(31) Groeger, O.; Gasteiger, H. A.; Suchsland, J.-P. *J. Electrochem. Soc.* **2015**, *162*, A2605−A2622.

(32) Itoh, T.; Sato, H.; Nishina, T.; Matue, T.; Uchida, I. *J. Power Sources* **1997**, *68*, 333−337.

(33) Cancado, L. G.; Takai, K.; Enoki, T.; Endo, M.; Kim, Y. A.; Mizusaki, H.; Speziali, N. L.; Jorio, A.; Pimenta, M. A. *Carbon* **2008**, *46*, 272−275.

(34) Zhu, Y.; He, X.; Mo, Y. *ACS Appl. Mater. Interfaces* **2015**, *7*, 23685−23693.

(35) Shin, B. R.; Nam, Y. J.; Oh, D. Y.; Kim, D. H.; Kim, J. W.; Jung, Y. S. *Electrochim. Acta* **2014**, *146*, 395−402.

(36) Wenzel, S.; Randau, S.; Leichtwei, T.; Weber, D. A.; Sann, J.; Zeier, W. G.; Janek, J. *Chem. Mater.* **2016**, *28*, 2400−2407.

(37) Wenzel, S.; Leichtweiss, T.; Weber, D. A.; Sann, J.; Zeier, W. G.; Janek, J. *ACS Appl. Mater. Interfaces* **2016**, *8*, 28216−28224.

(38) Sakuda, A.; Hayashi, A.; Tatsumisago, M. *Chem. Mater.* **2010**, *22*, 949−956.

(39) Jung, Y. S.; Lu, P.; Cavanagh, A. S.; Ban, C.; Kim, G. H.; Lee, S. H.; George, S. M.; Harris, S. J.; Dillon, A. C. *Adv. Energy Mater.* **2013**, *3*, 213−219.

(40) Gaberscek, M.; Moskon, J.; Erjavec, B.; Dominko, R.; Jamnik, J. *Electrochem. Solid-State Lett.* **2008**, *11*, A170−A174.

(41) Atebamba, J. M.; Moskon, J.; Pejovnik, S.; Gaberscek, M. *J. Electrochem. Soc.* **2010**, *157*, A1218−A1228.

(42) Kang, E.; Jung, Y. S.; Kim, G. H.; Chun, J.; Wiesner, U.; Dillon, A. C.; Kim, J. K.; Lee, J. *Adv. Funct. Mater.* **2011**, *21*, 4349−4357.

(43) Haruyama, J.; Sodeyama, K.; Han, L.; Takada, K.; Tateyama, Y. *Chem. Mater.* **2014**, *26*, 4248−4255.

(44) Chen, J. G.; Basu, P.; Ng, L.; Yates, J. T. *Surf. Sci.* **1988**, *194*, 397−418.

(45) Brodd, R. J. *Batteries for Sustainability: Selected Entries from the Encyclopedia of Sustainability Science and Technology*; Springer: New York, 2012; pp 336.

(46) Xu, K. *Chem. Rev.* **2004**, *104*, 4303−4417.

(47) Choi, N. S.; Ha, S. Y.; Lee, Y. W.; Jang, J. Y.; Jeong, M. H.; Shin, W. C.; Ue, M. *J. Electrochem. Sci. Technol.* **2015**, *6*, 35−49.

(48) Li, Y.; Zhou, W.; Chen, X.; Lu, X.; Cui, Z.; Xin, S.; Xue, L.; Jia, Q.; Goodenough, J. B. *Proc. Natl. Acad. Sci. U. S. A.* **2016**, *113*, 13313−13317.

(49) von Zamory, J.; Bedu, M.; Fantini, S.; Passerini, S.; Paillard, E. *J. Power Sources* **2013**, *240*, 745−752.